Journal of the European Ceramic Society 45 (2025) 116978

Contents lists available at ScienceDirect

Journal of the European Ceramic Society

journal homepage: www.elsevier.com/locate/jeurceramsoc

Mechanical and thermal properties as a function of matrix composition of all-oxide ceramic matrix composites fabricated by a sequential infiltration process

F. Lindner *, G. Puchas, F. Wich, S. Hariri, S. Schafföner

Chair of Ceramic Materials Engineering, University of Bayreuth, Prof.-Rüdiger-Bormann-Str. 1, Bayreuth 95447, Germany

ARTICLE INFO

Keywords:
Ceramic matrix composites
All-oxide
Prepreg
Slurry infiltration
Lamination process

ABSTRACT

The microstructural design of matrices for all-oxide ceramic matrix composites (Ox/Ox) with damage tolerant fracture behavior is challenging. Therefore, the potential use of different matrix materials might be limited even though they appear to offer advantageous functional properties, such as thermal insulation or corrosion resistance. In this study, we investigated the hypothesis of simultaneously adjusting mechanical and functional properties by separate matrix phases within and between the fiber bundles in Ox/Ox. A sequential infiltration process was used to manufacture Ox/Ox with an alumina-zirconia matrix phase (high damage tolerance) and a mullite-alumina matrix phase (thermal insulation). The effect on the mechanical and thermal properties was governed by the infiltration sequences. A property combination was achieved for either the mechanical or the thermal behavior. This was due to a shear-induced mixing of the matrix phases during the lamination process, which renders it difficult to achieve distinctly separated matrix phases within the composite.

1. Introduction

Ceramic matrix composites (CMC) are a material class designated for the use in high-temperature structural applications. Contrary to monolithic ceramics, catastrophic failure under mechanical overload or thermal shock is avoided by combining ceramic fibers with a ceramic matrix, yielding a material with damage tolerant fracture behavior. CMCs can be differentiated according to their material composition, which is usually uniformly based on non-oxide or oxide ceramics. All-oxide ceramic matrix composites (Ox/Ox) comprise oxide fibers as well as an oxide matrix, which renders them inherently oxidation stable. This oxidation stability and their fairly simple production processes are the main advantages compared to non-oxide CMCs, such as silicon carbide (SiC) or carbon (C) fiber reinforced C or SiC (C/C, C/SiC, SiC/SiC). This makes Ox/Ox favorable candidates for the use in oxidizing and potentially also in combustion environments, such as in aircraft engines or as furnace components [1–3]. Charging racks or burner nozzles made of Ox/Ox have already been in use for several years and show excellent performance compared to alloys, which are usually used for those applications [4]. However, detrimental mechanisms, such as water vapor or hot gas corrosion, are still a major concern and therefore subject of research to improve the material lifetime and to enable a wider field of applications [5–8].

Currently, only two high-performance oxide fibers for structural applications are commercially available, consisting of α-alumina (Nextel™610) and mullite-alumina (Nextel™720). Both fibers are provided by 3 M (USA). Their maximum use temperature is designated to be 1000 °C and 1150 °C, respectively, according to the manufacturers test standards [9]. In order to achieve a damage tolerant fracture behavior for CMCs, two material concepts can be chosen, i.e. weak interface composites (WIC) or weak matrix composites (WMC) [10]. The WIC concept is mostly used for non-oxide CMCs, with the necessity of a fiber coating that generates a weak interface between the fibers and the matrix to prevent crack propagation into the fiber. By contrast, the WMC strategy was specifically developed for Ox/Ox and is based on a matrix weakened due to a high amount of porosity. This porosity reduces the level of crack energy of the matrix well below that of the monolithic fiber, which leads to crack branching and deflection at pores and fibers, rather than crack propagation into the fiber, rendering a fiber coating obsolete [11]. Several research institutes and companies have developed Ox/Ox according to the WIC concept [12–19] and the WMC strategy [1,4,20–30] over the last decades.

For the matrix design of WMC, the matrix composition, the particle size and the porosity as well as the resulting sintering activity are of

* Corresponding author.
E-mail address: felix.lindner@uni-bayreuth.de (F. Lindner).

https://doi.org/10.1016/j.jeurceramsoc.2024.116978
Received 22 August 2024; Received in revised form 19 September 2024; Accepted 7 October 2024
Available online 9 October 2024

major interest. For example, to avoid corrosion, a more resistant matrix material, e.g. zirconia (ZrO_2) or yttria/yttrium aluminum garnet (Y_2O_3, YAG) [31,32], and a denser matrix, at least on the surface, might be favored [33,34]. On the other hand, for improved thermal insulation, matrix and fiber materials with a lower thermal conductivity, such as mullite, as well as an increased matrix porosity are of interest. These performance driven requirements, however, must not interfere with the microstructural requirements according to the WMC concept [35].

Key issues regarding the compatibility of the fiber and the matrix are the thermal expansion coefficients and a low diffusion rate at high temperatures, in order to reduce the risk of material damage during processing or service. As mentioned above, the variety of oxide fibers is quite limited, thus limiting the choice of matrix materials as well. Furthermore, the generation of a matrix system with a damage-tolerant fracture behavior can be challenging as not all oxide powders fulfill the desired sintering properties for WMC. As the matrix particles must enable infiltration of the fiber bundles (single fiber diameter of 11–14 μm), powders with a small particle size, favorably in the submicron range, are necessary [10]. In turn, due to their small size and high surface area, sintering activity might exceed the desired level, whether during fabrication or during long-term use, causing extensive densification and reduced damage tolerance [1]. By contrast, off-axis mechanical properties can be enhanced by stronger sintering [36], which requires a compromise for the material design depending on the respective application.

Therefore, the combination of different matrices in one composite appears intriguing to allow both damage tolerant fracture behavior and increased functional properties for specific applications. For example, Guglielmi et al. [21] developed a manufacturing process that includes two slurry infiltrations, yet in their case it was motivated by processing aspects. While an ethanol-based slurry served for the first infiltration, a paraffin-based suspension was applied for the second infiltration, which was rather a lamination. The second infiltration allowed joining of the prepregs in the green state by heating with good adhesion between the prepreg plies throughout the whole process. In another study, Puchas et al. [37] also published a double-step infiltration process applicable for oxide fiber fabrics. The motivation for their process was to facilitate a homogeneous infiltration of a fiber preform by a slurry, even though the fiber bundles were under compression due to a vacuum infiltration process. They showed that pressureless pre-infiltration of fabrics with a slurry of low solid loading and subsequent drying spread the fiber bundles and thereby improved the homogeneity of the second infiltration which was performed with the same slurry, yet with increased solid loading. Due to the improved infiltration quality of the fiber bundles, the mechanical strength increased with this double-infiltration process.

Thus, the aim of the present study was the fabrication of Ox/Ox by applying a sequential infiltration process, that yields two distinct matrix phases within the fiber bundle (intrabundle) and between them (interbundle). The matrix phase compositions were alumina-zirconia, with proven suitability for WMC-Ox/Ox [38–41], and mullite-alumina, which yields a lower mechanical strength but increased thermal insulation capability of the composite [42]. By investigating the mechanical and thermal properties of the Ox/Ox with uniform and non-uniform matrix phases, the properties as a function of phase composition and possible beneficial effects of the combined usage of matrix phases were assessed. Potential drawbacks from the sequential infiltration in comparison to the single-step infiltration were also investigated by the fabrication of single and sequentially infiltrated Ox/Ox with uniform matrix phase composition.

2. Material and methods

2.1. Slurry preparation

The Ox/Ox were fabricated according to a prepreg route (Fig. 1), which has already been extensively described [39].

The slurry compositions are given in Table 1. For the alumina-zirconia slurry, a coarser alumina powder (CT 3000 SG, Almatis, Germany) and a finer alumina powder (TM-DAR, Taimei Chemicals, Japan) were used as well as a zirconia powder (TZ-3Y-E, Tosoh, Japan). By contrast, the mullite-alumina slurry contained mullite (SYMULOX M672, Nabaltec, Germany) and the finer alumina powder. The slurries, henceforth referred to as AZ and MA slurry, had solid contents of 63 wt % and 60 wt%, respectively. Different sodium polyacrylate-based dispersants were used, namely D1 (Sokalan PA15, BASF, Germany) for the AZ slurry and D2 (BYK-155/35, BYK-Chemie GmbH, Germany) for the MA slurry as well as glycerol as a hygroscopic substance. The glycerol and dispersant content of the MA slurry were determined based on a rheological trial of the conditioned slurry, and therefore vary from the AZ slurry. Drum milling for 2–3 days with zirconia beads (diameter 3 mm) led to homogeneous slurries with a maximum particle size of

Table 1
Composition of the slurries used in this work (*relative to the solid content, **relative to the liquid content).

	Alumina-zirconia slurry (AZ)	Mullite-alumina slurry (MA)
Powder [wt%]	63	60
Alumina coarse [%]	70	-
Alumina fine [%]	5	10
Zirconia [%]	25	-
Mullite [%]	-	90
Dispersant [wt%*]	1.5 (D1)	3.0 (D2)
Glycerol [wt%*]	26	32
Xanthan gum [wt%]**	0.2	0.2
Water	remaining	remaining

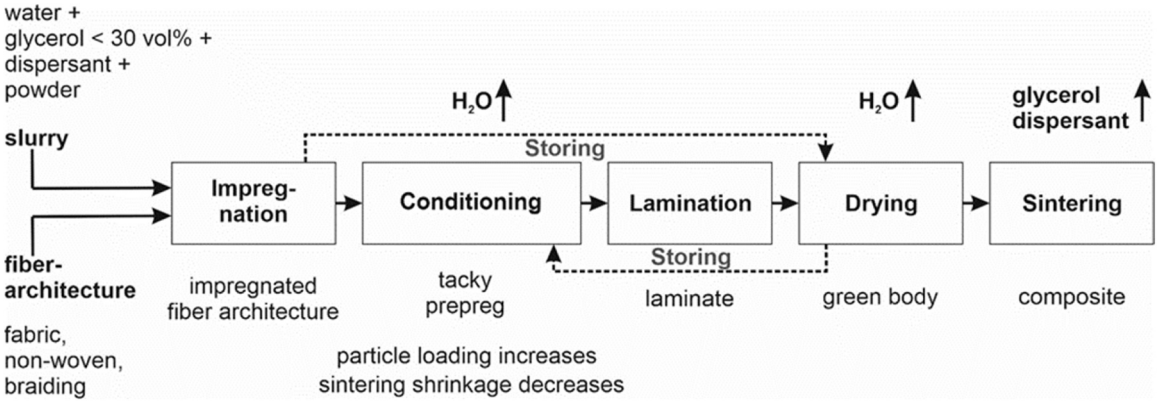

Fig. 1. Flow chart of the prepreg based fabrication process for Ox/Ox [39].

<6 μm. After milling, 0.2 wt% xanthan gum (Carl Roth AG, Germany) relative to the liquid phase were added as a thickening agent. To avoid clumping, the xanthan gum was dissolved in deionized water (xanthan content 1 wt%) [43,44], which led to the solid content shown in Table 1.

2.2. Prepreg fabrication

Nextel™720 fabrics (EF-19; 3 M Corporation, USA) with 110×110 mm^2 in size were infiltrated with the slurries using a brush. The slurry volume was adjusted with a doctor blade system. For the first step of the sequential infiltration process, the blade height was set to 300 μm as this yielded prepregs with fully infiltrated fiber rovings and low excessive residual slurry (Fig. 2). Subsequently, the infiltrated fabrics were conditioned in a climatic chamber (305SB / +10 IU, Weiss, Germany) at 65–67 %RH and 25 °C for 16 h. Before the second infiltration, the prepregs were put into a drying chamber (FDL 115, Binder, Germany) at 50 °C for 1.5 h and 60 °C for 1 h which led to a leather-like prepreg state. For the second infiltration, the slurry was applied on each side of the prepregs and the infiltration was facilitated with a degassing roller. After adjusting the slurry volume with a doctor blade system of 800 μm, the prepregs were put into the climatic chamber for a second conditioning step at 25 °C and 66 %RH for 16 h. Based on our hypothesis, the first infiltration yielded the intrabundle matrix, the second created the interbundle matrix. Sequential infiltration was performed with uniform and non-uniform slurry compositions, i.e. using the same slurry for the first and the second infiltration or different slurries, respectively. For comparison, prepregs with uniform matrices were also fabricated by a single-step infiltration (blade height 900 μm), which corresponded to the standard fabrication method depicted in Fig. 1.

The samples are denoted according to their infiltration sequence, e.g. AZ represents a single step infiltrated Ox/Ox with AZ slurry and AZ-MA stands for a sequentially infiltrated Ox/Ox with AZ (first step) and MA slurry (second step). This gives the following sample denotations (Table 2).

After conditioning, the prepregs were stacked and carefully laminated with a cold roll laminator. Two plates for each prepreg system were fabricated with a compression level of up to 39 % and 44 % in fiber volume content, comprising four and eight fabric layers, respectively. This was necessary in order to fulfill the respective standards for the mechanical testing regarding the ratio of the support span to the sample thickness. Subsequently, the laminates were put in a drying chamber at 60 °C for 2 h and 100 °C for 16 h. Finally, the laminates were sintered at 1225 °C for 2 h in a sintering furnace (LH 60/14, Nabertherm, Germany) in air, which in the past has proven to yield sufficient sintering for both matrix phases.

Table 2
Sample denotations in this work.

		Second infiltration		Single-step infiltration
		AZ	MA	-
First infiltration	AZ	AZ-AZ	AZ-MA	AZ
	MA	MA-AZ	MA-MA	MA

2.3. Characterization methods

The particle size distribution of the slurries was analyzed with a laser granulometer (PSA 1190 L/D, Anton Paar, Austria) and the viscosity was measured by means of a rotational rheometer (MCR702 MultiDrive, Anton Paar, Austria) with a cone-plate-system (25 mm, 2°) at laboratory conditions (22 °C). To analyze the effect of the sequential infiltration on the processing properties of the prepregs, our tack testing method was implemented [45]. This method monitors the rebound behavior of prepreg stacks (30×30 mm^2) after compression to a target fiber volume content, in this case 39 %, within a rheometer setup (plate-plate-geometry, 25 mm). Prepreg samples were fabricated according to the process described above (Fig. 1). Mechanical testing of the Ox/Ox was performed with a universal testing machine (Z050TEW, ZwickRoell Testing Systems GmbH, Austria) to determine the 3-point flexural strength (DIN EN ISO 17138) and interlaminar shear strength (ILSS; DIN EN 658–5). The support span was set to 50 mm and 15 mm, respectively. Tests were conducted with a 5 kN load cell and a cross-head speed of 1 mm/min. At least six samples (70x10x1.85–2.08 mm^3; 30x10x3.29–3.54 mm^3) were tested for each Ox/Ox. The open porosity and the bulk density ρ were measured by water immersion (Archimedes´ principle, DIN EN 1389). The microstructure was analyzed by scanning electron microscopy (SEM; Sigma 300 VP, Zeiss, Germany), using an SE- and BSE-detector and an accelerating voltage of up to 20 kV. To analyze the element distribution in the composite, energy dispersive X-ray spectroscopy (Octane Elect Silicon Drift Detector, AMETEK, USA) was performed. The thermal diffusivity α was measured by laser flash analysis (LFA; LFA 427, Netzsch, Germany) with a laser voltage of 400 V and a pulse length of 0.8 s. The specific heat capacity c_p was measured by differential scanning calorimetry (DSC; DSC 204, Netzsch, Germany) with a sapphire standard sample up to 600 °C. Thermal conductivity λ was calculated according to Eq. 1. All test samples were extracted from the Ox/Ox with a water-cooled diamond wire saw (Type 6234, Well, Germany). Grinding and polishing was performed, if necessary.

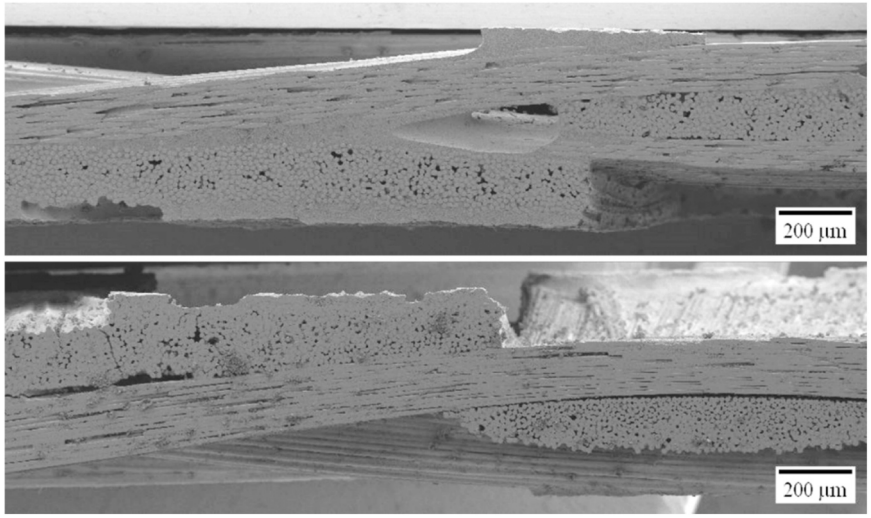

Fig. 2. SEM images of sintered single prepreg plies after the first infiltration step with a doctor blade height of 300 μm (top: AZ; bottom: MA).

$$\lambda = \alpha \times c_p \times \rho \quad (1)$$

3. Results and discussion

3.1. Slurry properties

The particle size distribution of the AZ and MA slurries is depicted in Fig. 3. The MA slurry clearly showed a narrower particle size distribution with a distribution width of 1.6 due to the lack of a small particle fraction compared to the AZ slurry (distribution width of 3.3). This lack of small particle fraction is caused by the larger primary particle diameter of the mullite compared to the alumina and zirconia, respectively. In our previous study [45], we discovered a negative effect of an increased particle size on the compression behavior of the prepregs in the lamination process. Yet, this impact was expected to be negligible in this work, as the particle size of the slurries differed by a smaller margin and even the largest particles were only half the fiber diameter.

In addition to the particle size, the slurry viscosity in the prepreg state, i.e. after conditioning, is a crucial property for the prepreg processing as well. As can be seen in Fig. 4, the flow behavior of the AZ and MA slurries in the conditioned state (25 °C, 66 %RH) was somewhat different. The MA slurry did not reach the desired high viscosity level of the AZ slurry at low shear rates and did not show a distinct shear thickening behavior above 30 1/s. This might lead to lower tackiness. Thus, fairly low compression levels of 39 % and 44 % for Ox/Ox with four and eight layers, respectively, were chosen in this work to reduce the effect of rebound [45]. In general, for the sequential fabrication process investigated in this work, the slurry systems that ought to be combined must have matching processing windows for the lamination, i.e. show satisfying rheological flow behavior at the same conditioning humidity.

3.2. Processing properties (tack measurement)

The results gained from the tack measurements of mini-laminates with four prepregs layers are depicted in Fig. 5 and Fig. 6. For an extensive explanation of the interpretation of the test results, interested readers are referred to our previous study [45]. In Fig. 5, the prepregs pre-infiltrated with the AZ slurry (AZ-AZ, AZ-MA) and the single-step infiltrated prepregs (AZ, MA) are compared. The maximum compression stress required to reach the targeted fiber volume content of 39 % ranged from approximately 2.4 to 3.1 kPa. The single step infiltrated MA sample exhibited the largest rebound in fiber volume content with 0.9 percentage points while AZ, AZ-AZ and AZ-MA samples showed a fairly identical rebound behavior and ended up with a rebound of 0.5 percentage points. In contrast to the AZ slurry pre-infiltration, the rebound

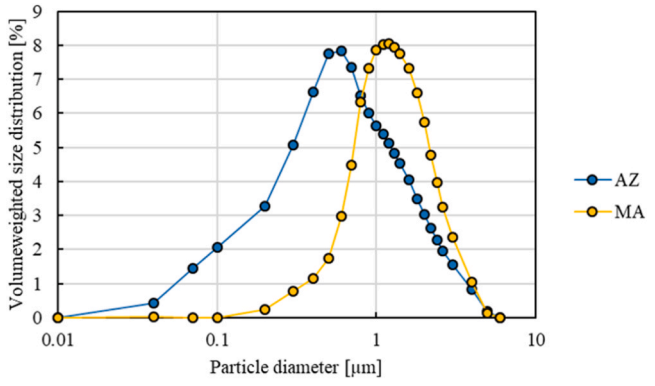

Fig. 3. Particle size distribution of the alumina-zirconia (AZ) and mullite-alumina (MA) slurries used to fabricate the Ox/Ox in this work. The MA slurry exhibited a narrower size distribution due to a lack of small particle fraction.

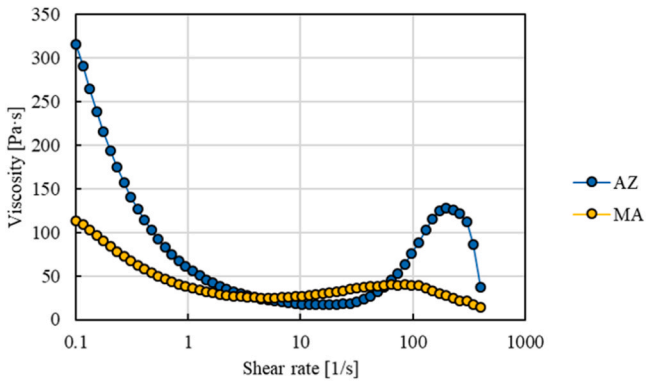

Fig. 4. Viscosity as a function of the shear rate of the AZ and MA slurries in the conditioned state (25 °C, 65.5%RH).

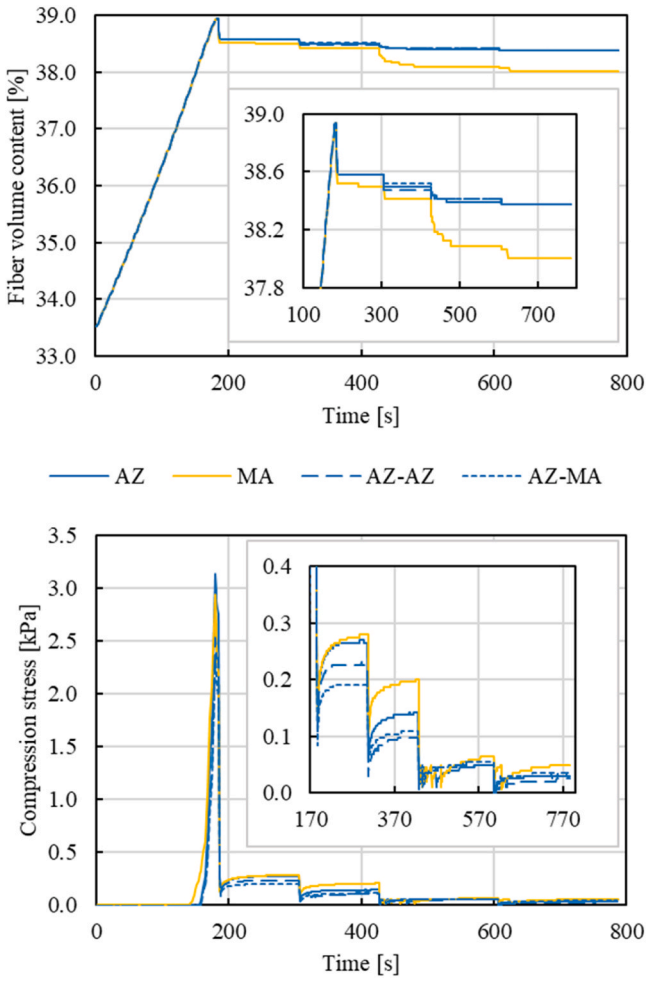

Fig. 5. Fiber volume content (top) and compression stress (bottom) as a function of the testing time for representative AZ, MA, AZ-AZ and AZ-MA samples (four prepreg layers) in the tack test.

of samples pre-infiltrated with the MA slurry (MA-AZ, MA-MA) was 0.6 to 0.7 percentage points (Fig. 6) and therefore somewhat higher, which can be attributed to the non-ideal flow behavior of the MA slurry.

Due to the already mentioned lower targeted compression level, the values obtained for compression stress and rebound for all samples were fairly low compared to previous tests [45] and deemed suitable for the lamination process. Furthermore, the variations noticed between the sequential and single-step infiltration were quite low. Therefore, the

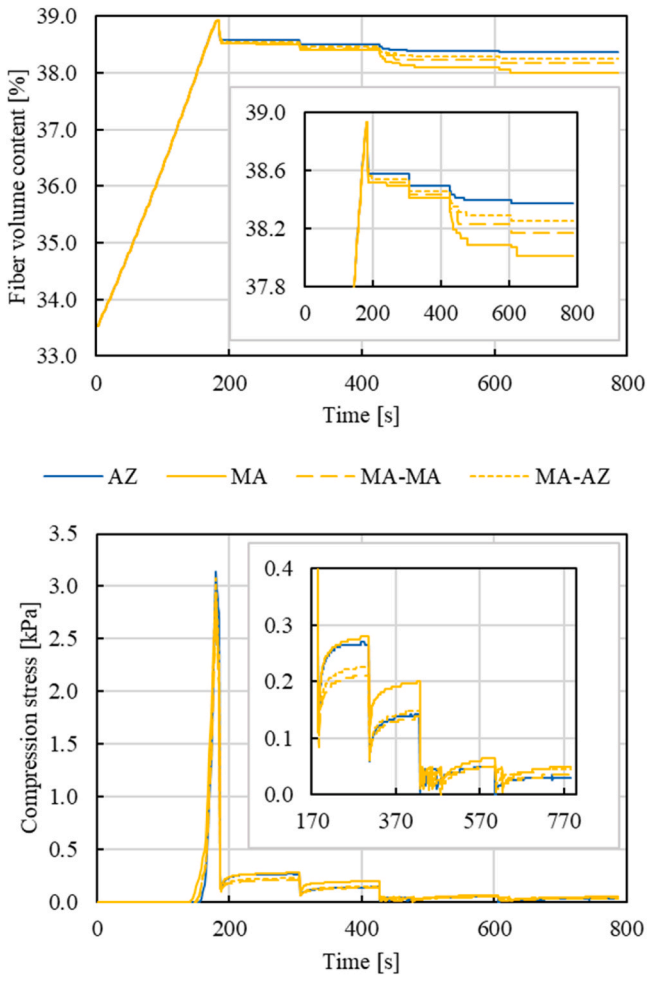

Fig. 6. Fiber volume content (top) and compression stress (bottom) as a function of the testing time for representative AZ, MA, MA-AZ and MA-MA samples (four prepreg layers) in the tack test.

results of this measurement method suggested that the sequential infiltration had no detrimental effect on the lamination process.

3.3. Ox/Ox properties

3.3.1. Porosity and fiber volume content

The fiber volume content as well as the open porosity of the Ox/Ox and the matrix are listed in Table 3 for Ox/Ox with four and eight fabric layers.

In general, laminates with higher fabric layer count show favorable volumetric arrangement due to the so called "nesting" of the fabric undulations of facing fabric layers [46]. However, to properly remove entrapped air between the prepreg plies, the prepreg stack must be submitted to some compression which is why the desired compression level of the samples with eight layers was set five percentage points higher than for the ones with four layers. Even though the lamination process was performed thoroughly, the Ox/Ox with four fabric layers exhibited a divergence of up to 3.1 percentage points from the tack test without any obvious correlation to the slurry systems involved. Even though no tack test were conducted for laminates with eight layers, the variation was lower as the maximum deviation from the initial compression level (44 %) was 2.8 percentage points without considering the intrinsic rebound. As described in our previous study [45], the tack measurement method is not able to emulate the actual fabrication to a full extent. Specifically, the shear forces are way higher in the laminator and lead to enhanced squeeze flow of the slurry. Furthermore, with

Table 3
Fiber volume content, open porosity and matrix porosity of the Ox/Ox with four and eight fabric layers.

	Layer count	Fiber volume content [%]	Open porosity [vol.%]	Matrix porosity [vol.%]
AZ	4	38.4	30.1	48.8
MA		36.4	31.1	48.9
AZ-AZ		36.6	31.3	49.4
MA-MA		35.2	31.3	48.3
AZ-MA		37.2	30.1	47.9
MA-AZ		38.0	30.5	49.2
AZ	8	42.8	30.0	52.4
MA		42.4	30.9	53.6
AZ-AZ		41.4	30.9	53.6
MA-MA		41.2	31.8	54.1
AZ-MA		42.5	30.0	52.2
MA-AZ		41.6	31.4	53.7

increasing prepreg size, the chance of misalignment between the plies, i.e. unfavorable positioning of undulations, is higher, which impedes compression and favors rebound. Additionally, for high compression forces, the compliance of the laminator setup adds uncertainty to the intended compression level. Hence, the fabrication process is inherently subjected to variations that are only partially present in the tack test and which lead to lower fiber volume contents in the final composite. For a distinct evaluation of the slurry systems and their respective processing properties, the results gained from the tack test should be considered.

As the fibers are fully dense, the open porosity is solely located in the matrix volume. Hence, only the matrix porosity was compared rather than the open porosity. As can be seen, the values of the matrix porosity varied by 0.6 to 1.2 percentage points within the same prepreg system when using single or sequential infiltration. Based on our experience, the matrix porosity fluctuates by up to 2 percentage points due to the fabrication process, which is why the differences shown in Table 3 are considered as negligible. In total, the matrix porosity was higher for samples with eight layers compared to the ones with four layers, which is also in line with our previous investigation [42]. This is due to the fact that a higher fiber volume content causes lower packing density of the matrix particles [47].

3.3.2. Microstructural analysis

In Fig. 7(a, b) the microstructures of the transition area from the intra- to interbundle matrix of the Ox/Ox with eight layers and uniform matrix compositions (AZ, MA) are shown. The major differences between the AZ and MA matrix were the particle size, as already discussed, and the sintering behavior. Sintering was qualitatively assessed by comparing the grinding planes of the fibers and the matrix. While the fibers seemed to protrude out of the AZ matrix (Fig. 7(a)) they were fairly in-plane with the MA matrix (Fig. 7(b)), indicating matrix failure of the AZ sample during the grinding process [38]. This lack of weakness for the MA sample was an indicator for potential incompatibility with the WMC concept.

The comparison of the microstructures of single-step (Fig. 7(a, b)) and sequentially infiltrated Ox/Ox (Fig. 7(c, d)) of uniform matrix phase composition revealed no noticeable difference between the two processing methods for AZ and MA samples. Thus, the sequential infiltration did not affect the microstructure. Even though a better infiltration of the fiber bundles in Fig. 7(d) compared to Fig. 7(b) might be observed, it was not representative for the whole sample.

The Ox/Ox fabricated by the sequential infiltration process with

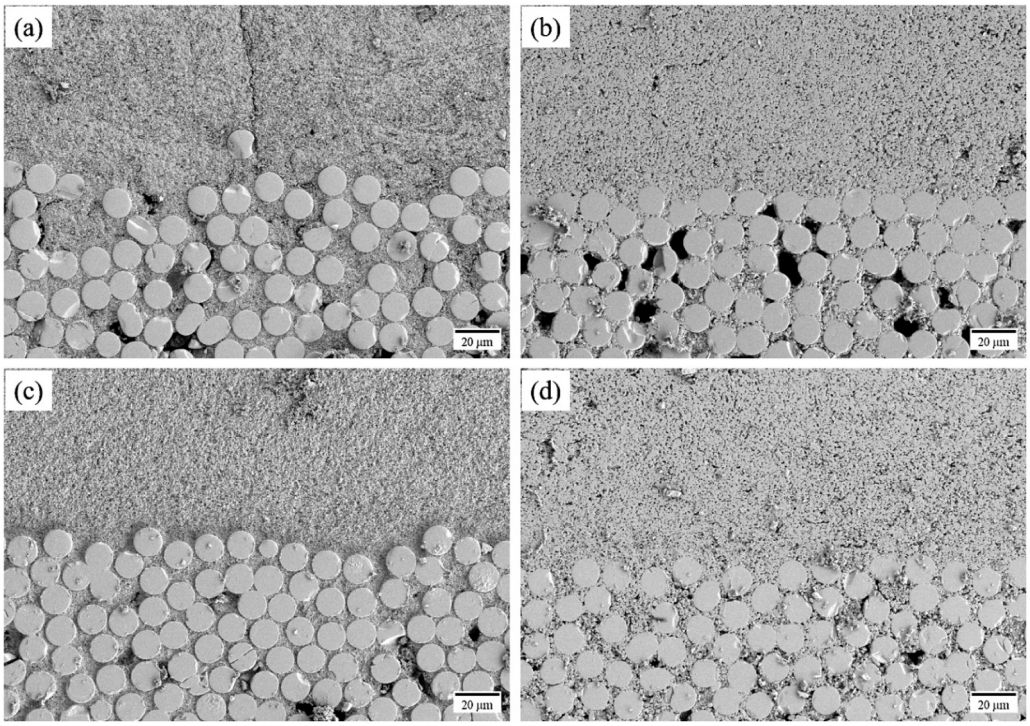

Fig. 7. SEM images (SE detector) of the microstructure of Ox/Ox with eight layers and the AZ (a), MA (b), AZ-AZ (c) and MA-MA matrix (d). Protruding fibers in (a) and (c) indicate a certain weakness of the AZ matrix while similar grinding planes for the fibers and the MA matrix in (b) and (d) imply higher matrix strength.

different matrix phase compositions were supposed to yield distinctly separated matrix areas within the microstructure, each exhibiting the aforementioned characteristics of the respective matrix phase, regarding particle size and sintering behavior. In order to visualize the elemental composition of the matrix phases, SEM images using the BSE detector and EDX spectroscopy were performed. As aluminum (from alumina) was present in both matrices and silica (from mullite) was found in the fiber and the matrix, zirconium (from zirconia) was chosen as the indicator for matrix phase mixing. Fig. 8 shows the BSE image and its corresponding EDX mapping for zirconium, where the light areas in the BSE image represent the higher atomic number element zirconium. It must be pointed out that in the following discussion about the mixing of the matrix phases zirconium is mentioned on behalf of the AZ matrix phase, which means that areas where zirconia was detected also comprise the corresponding volume fractions of alumina particles of the AZ phase. This could be derived from Fig. 8(b, c), which showed a distinct phase separation between the zirconium containing AZ phase and silicon containing MA phase.

The microstructures of AZ-MA and MA-AZ Ox/Ox samples with eight (Fig. 9(a) and (b)) and four fabric layers (Fig. 9(c) and (d)) are provided in the following. A low magnification was chosen to give an overall impression of the sample cross sections.

For both samples with eight layers, as intended, the majority of fiber bundles still contained the intrabundle matrix phase, i.e. the matrix phase from the first infiltration step, while the interbundle matrix phase composition (second infiltration) was mainly located in the interbundle area. Nevertheless, some fiber bundles were partially infiltrated by the interbundle matrix phase, especially in the outer region of the bundle. Moreover, the interbundle areas showed considerable commingling of both matrix phases (Fig. 10). This commingling could be traced back to excess slurry from the first infiltration (Fig. 2) and shear-induced slurry flow in the lamination step. Additionally, the shear forces in the lamination step might have also squeezed out some intrabundle slurry into the interbundle area. This led to the overall impression, that the initial intrabundle matrix phase was somewhat dominant throughout the composite.

The same conclusion can be drawn for the Ox/Ox with four fabric layers (Fig. 9(c, d)), yet the comingling of the inter- and intrabundle matrix phases was more intense and also involved more of the fiber bundles. As already discussed, due to the less favorable fabric layer arrangement, the shear forces for the Ox/Ox with four layers were higher than for the Ox/Ox with eight layers. Due to the excess amount of

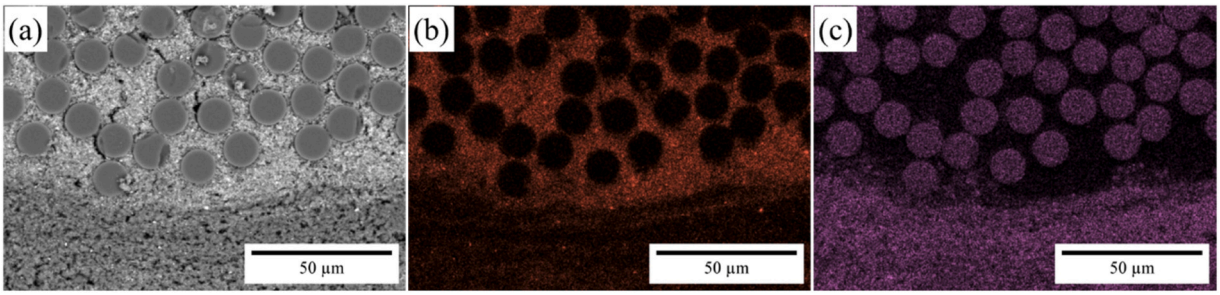

Fig. 8. SEM image (BSE detector, (a)) as well as EDX mappings for zirconium (b) and silicon (c) of Ox/Ox with eight layers and the AZ-MA matrix. Light areas in (a) and red colored areas in (b) correspond to the element zirconium and therefore to zirconia.

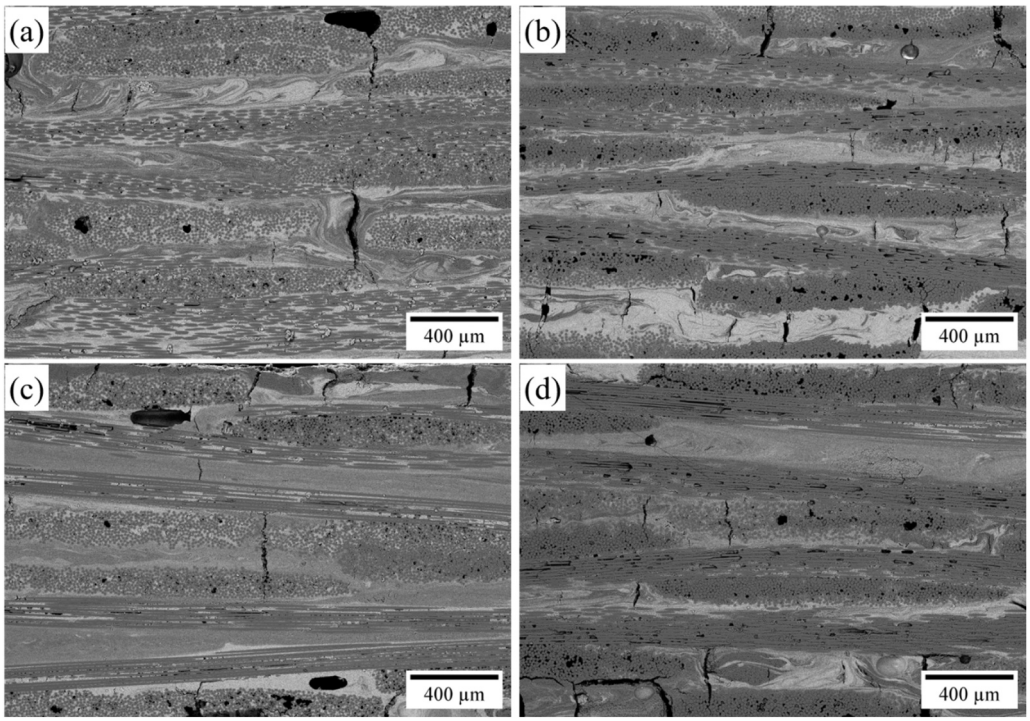

Fig. 9. SEM images (BSE detector) of Ox/Ox with the AZ-MA and MA-AZ matrix comprising eight (a, b) and four fabric layers (c, d). A considerable commingling of matrix phases was observed for all samples, with the intrabundle matrix phase appearing dominant throughout the composite in all cases.

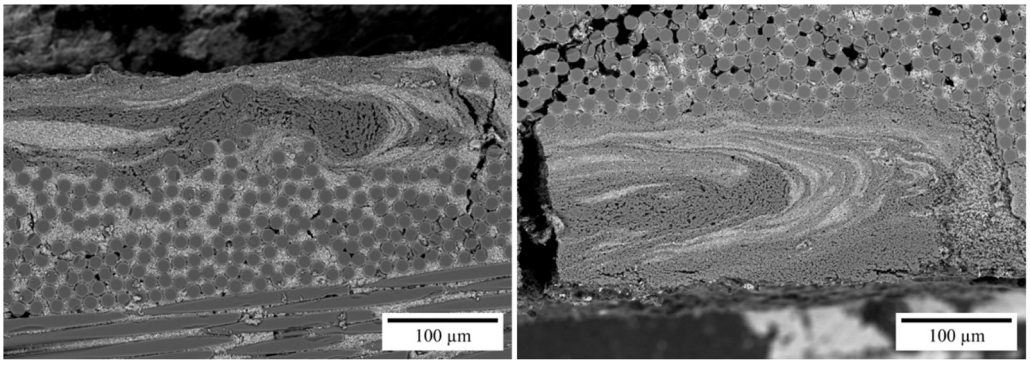

Fig. 10. SEM images (BSE detector) of the AZ-MA Ox/Ox showing considerable commingling of matrices in the interbundle areas.

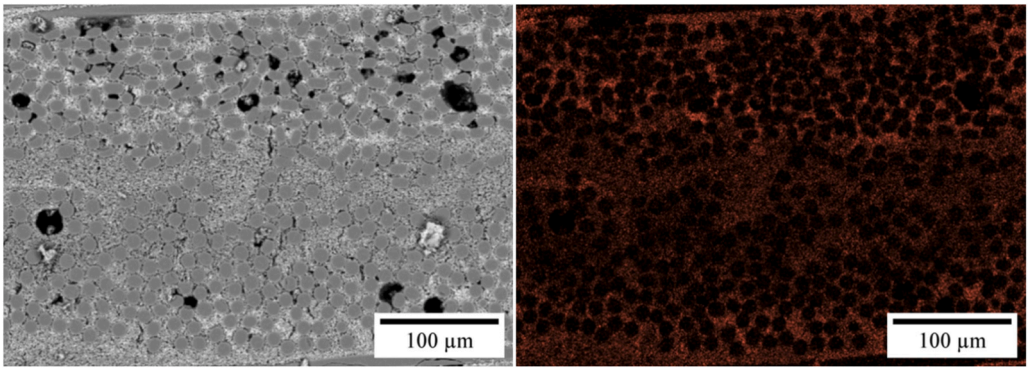

Fig. 11. SEM image (BSE detector) and EDX mapping of zirconium of the AZ-MA Ox/Ox showing the indistinguishable transition area between the fiber bundles of two prepreg plies in the composite.

intrabundle matrix phase, a quasi-continuous transition from the inside to the outside of the fiber bundle with a high amount of intrabundle matrix phase present around the bundle was detected. This made the identification of intra- and interbundle matrix phase almost impossible, especially at areas of close contact between the fiber bundles of two prepreg plies (Fig. 11).

Assessing representative transition areas from intra- to interbundle for each sample by EDX spectroscopy (Fig. 12) a higher flowability of the zirconium (i.e. zirconia) was suggested, if it was infiltrated first. This might be attributed to the different flow behavior of the slurries during the lamination step, with the MA matrix phase showing less intense flow especially when being present in the bundle. This fits well with previous observations, that can be accounted to the higher particle size and the steric hindrance that is accompanied therewith, especially inside the fiber bundle. Fig. 12 also supported our previous considerations, i.e. that the mixing of matrix phases was more intense when higher shear forces were present during the lamination step (Fig. 12 (c, d)). The extent to which this mixing of matrices affected the mechanical properties and failure behavior as well as the thermal properties is discussed in the following sections.

3.3.3. *Mechanical properties*

The flexural strength and Young's modulus of the fabricated Ox/Ox derived from the 3-point flexural tests are plotted in Fig. 13, normalized to a fiber volume content of 38% for better comparison. It has to be noted that these results were obtained for Ox/Ox with four layers, i.e. with significant mixture of matrix phases as discussed in the previous section. The error bars show the 99% confidence interval of the seven samples tested for each Ox/Ox.

Within each uniform matrix composition, i.e. AZ and AZ-AZ as well as MA and MA-MA, the flexural strength of 186 and 178 MPa as well as 106 and 102 MPa did not differ statistically, indicating no detrimental effect of the sequential infiltration. However, this did not translate to the Young's modulus for samples with the AZ matrix, as the confidence intervals of both mean values (53 and 56 GPa) did not overlap, thereby implying a higher stiffness due to the sequential infiltration. Further investigations are necessary to explain the reason behind this difference in Young's modulus. In accordance to the flexural strength and the microstructural observations, the samples with the MA matrix (63 and 59 GPa) statistically exhibited the same Young's modulus.

These results underline the initially claimed lack of mechanical strength provided by the MA matrix in comparison to the AZ matrix. While the high level of sintering led to a high strength within the MA matrix, as already identified in the microstructural analysis, and a higher Young's modulus in the composite, it was not able to provide a high 3-point bending strength in the composite. This appears reasonable, as a higher strength increases the probability of crack propagation from the matrix into the fiber. Additionally, since the average grain size of the MA matrix is significantly higher than that of the AZ matrix, larger particle diameters reduce the number of particles between the fibers, which decreases mechanical decoupling of the fibers. Both aspects led to a failure at lower strength for the MA matrix containing composites.

Comparing the non-uniform matrix system AZ-MA with the matrix systems AZ-AZ and MA-MA, it can be seen that the strength of 144 MPa for AZ-MA was clearly different, ranging fairly in the middle. At the same time, the Young's modulus of 61 GPa corresponded well with the MA-containing matrix systems (MA, MA-AZ, MA-MA) and thereby exceeded AZ and AZ-AZ. In turn, when both matrices were used in the opposite order, i.e. first infiltration with the MA slurry and second infiltration with the AZ slurry, the results (MA-AZ) differed significantly. While the Young's modulus (60 GPa) was in line with the other MA-containing matrix systems, the flexural strength of 89 MPa was the lowest recorded in this study.

Including the stress-strain-relation of representative specimens for each Ox/Ox system (Fig. 14) in the discussion, the AZ-MA matrix stands out again. While the MA, MA-MA and MA-AZ as well as AZ and AZ-AZ matrices exhibited rather similar stress-strain relations with regard to maximum and residual strength, the AZ-MA matrix was clearly situated in between and showed a gradual strength degradation after surpassing the maximum load instead of an immediate drop-off.

As discussed in the previous section, the microstructures of Ox/Ox laminated with four prepreg layers showed intense mixing of inter- and

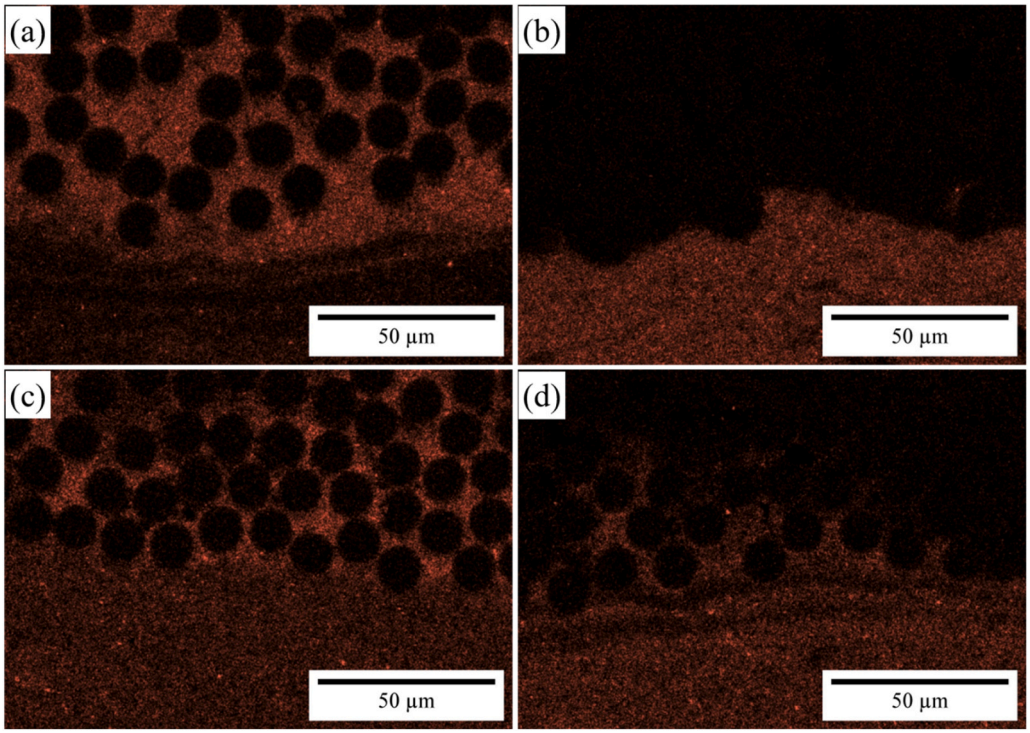

Fig. 12. EDX mappings of zirconium of Ox/Ox with the AZ-MA and MA-AZ matrix comprising eight (a, b) and four fabric layers (c, d). A higher mobility of the zirconium was suggested, if it was initially present in the intrabundle area.

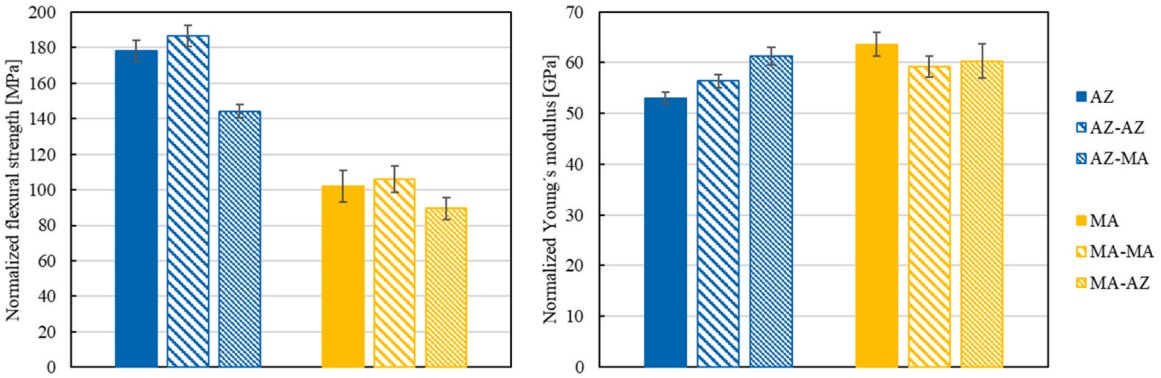

Fig. 13. Normalized 3-point flexural strength (left) and Young's modulus (right) for all Ox/Ox with four layers fabricated in this work (normalized to a fiber volume content of 38%). The error bars show the 99% confidence interval of the seven samples tested for each Ox/Ox.

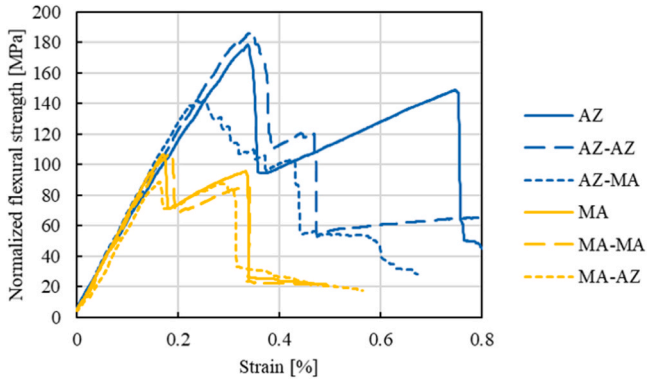

Fig. 14. Normalized stress-strain-behavior of representative samples for all Ox/Ox with four layers fabricated in this work (normalized to a fiber volume content of *38 %*); the curve of the Ox/Ox with AZ-MA matrix exhibited a unique stress-strain-behavior.

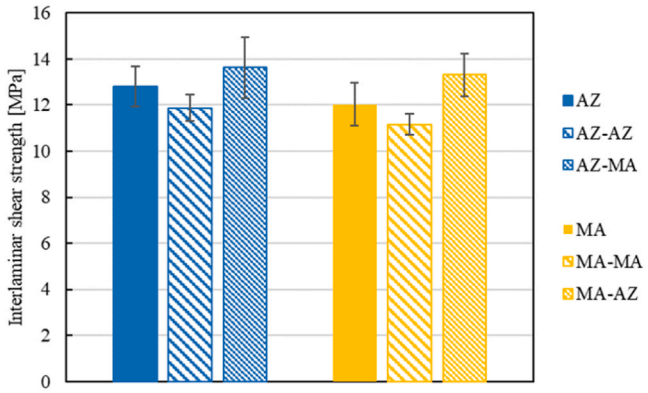

Fig. 15. Interlaminar shear strength for all Ox/Ox with eight layers fabricated in this work. The error bars show the *99 %* confidence interval of the seven samples tested for each Ox/Ox.

intrabundle matrices, with the intrabundle matrix being dominant throughout the composite. The mechanical tests were in line with this assessment. If the AZ-MA sample is considered to partially contain MA matrix phase within the fiber bundles and a highly mixed, AZ-dominated interbundle matrix phase, the decrease in strength and increase in stiffness, both governed by the matrix within the fiber bundle, is plausible. The unique stress-strain-relation after failure might be attributed to the microstructure that resulted from the sintering between the mullite and zirconia particles within and around the fiber bundle (Fig. 12 (c)) and should be assessed in more detail in future works. In contrast, the microstructure of the MA-AZ sample was the exact opposite of the AZ-MA sample. With MA as the dominating matrix phase, the addition of highly sintering active zirconia might have led to even stronger bonding between the matrix particles. Therefore, as the MA matrix has already been deemed non-ideal for the WMC concept, the strength of the MA-AZ Ox/Ox dropped even further.

These results showed that the AZ-MA composite offered a compromise between the higher strength of the AZ and the higher stiffness of the MA matrix, whereas the MA-AZ composite exhibited a lack of benefit from the matrix combination. Hence, it can be concluded that the increased sintering activity of the mullite particles was the dominating effect that governed the mechanical properties of the composite. When their presence within the fiber bundle was limited, the initially high strength and damage-tolerance of the AZ matrix was at least partially maintained together with an increased Young's modulus.

In Fig. 15 the interlaminar shear-strength (ILSS) of the Ox/Ox with eight layers is depicted. As already discussed, the microstructure of these Ox/Ox differed somewhat to the ones with four fabric layers, which is why they were assessed separately. Yet, as the ILSS is a matrix-dominated property and interbundle areas exhibited commingling of matrix phases in both cases, i.e. for composites with four and eight fabric layers, the results obtained should be valid for both.

Comparing the uniform matrices AZ (12.6 MPa) and MA (12.0 MPa), no significant difference was determined, irrespective of a single-step or sequential infiltration process (AZ-AZ, MA-MA), even though the mean values of the sequential infiltration were somewhat lower. In turn, the mean values of 13.5 MPa obtained for the non-uniform AZ-MA and MA-AZ matrices were higher than for AZ and MA matrices. As the tests showed no statistical significance, the ILSS must be seen as independent of the investigated matrix compositions and no beneficial or detrimental impact on the composite behavior was be attained. This is due to the fact that the interlaminar shear strength is mostly governed by the matrix porosity [38], which was very similar for all samples.

As we initially expected, the mechanical properties did improve for the Ox/Ox with AZ-MA matrix with respect to the pure MA matrix-based Ox/Ox. However, as the majority of the matrix is postulated to be represented by the intrabundle matrix phase for Ox/Ox with four layers, the fraction of mullite was expected to be small, so that the Ox/Ox performance might rather be seen as an AZ matrix Ox/Ox with reduced mechanical properties than a MA matrix composite with increased performance. In order to compare the obtained results with the ones from previous publications, it has to be mentioned that the mechanical properties are influenced by several factors. These factors include the fiber volume content, the fabric type used, the matrix composition, the porosity and the sintering program as well as the material concept and the testing procedure itself. In Table 4 an overview of mechanical properties published for Ox/Ox with Nextel™720 fabrics is given.

Table 4
Previously reported mechanical properties for Ox/Ox with Nextel™720 fabrics (*: weak interface composite).

Source	Matrix	Porosity [vol.%]	Fiber volume content [%]	Flexural strength [MPa]	Young's modulus [GPa]	ILSS [MPa]
This work	alumina, zirconia, mullite	30	37.2–42.5	144	61	13.5
[48]	alumina	20.7	50.8	180	80	12.5
[4]	alumo-silicate	30–35	35–40	150–200		12
[28]	alumina-silica	34.9	36.5	81.5	60.5	4.1
[49]*	SiOC, silica	16	48	213	59	
[50]	mullite, alumina	23.4	42.4	177	60	7

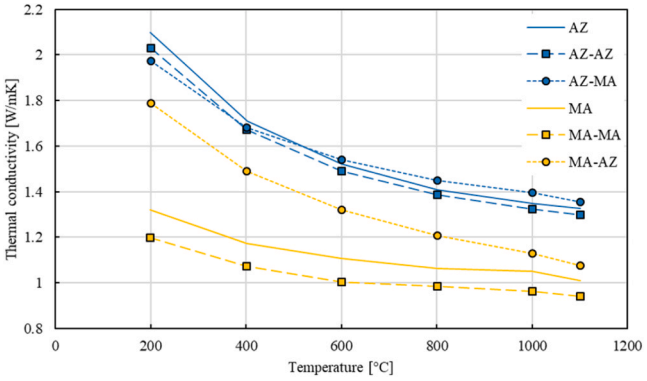

Fig. 16. Thermal conductivity as a function of the temperature for all Ox/Ox systems with four layers.

3.3.4. Thermal properties

The calculation of the thermal conductivity revealed the temperature function depicted in Fig. 16. The results were lower than previously reported [42] but also showed variations in sample porosity. In Table 5 the values obtained for the thermal diffusivity α, thermal conductivity λ and the specific heat capacity c_p at 1000 °C are given together with the thickness and density of the samples. Specific heat capacity measurements were only performed up to 600 °C, the values for higher temperatures were extrapolated based on previous measurements that were carried out up to 1000 °C [42]. The AZ-AZ and MA-MA samples were not measured separately, instead the specific heat capacity of the AZ and MA samples were used.

As expected, the results clearly showed that the best thermal insulation capability, i.e. the lowest λ, was obtained with the MA and MA-MA matrices with values ranging from 1.3 to 1.0 and 1.2 to 0.9 W/mK, respectively. Variations between the two matrices were accounted to the small sample size for the α-and c_p-measurements (10×10 mm^2 and diameter <5 mm, respectively) and the large effect of porosity variations for these small samples. The MA-AZ sample showed an intermediate behavior between the AZ and MA matrices (1.8 to 1.1 W/mK), but with a higher drop over the temperature range, while the AZ-MA Ox/Ox was in the range of 2.0 to 1.3 W/mK and thereby not distinguishable from AZ and AZ-AZ, indicating no contribution of the MA matrix content.

These results were well in line with the results and considerations so far, which are based on the presence of highly commingled matrix phases in the interbundle and partially intrabundle area, with the initial intrabundle matrix being dominant throughout the composite. As the amount of alumina in the MA matrix phase is increased due to the mixing with the AZ matrix phase in MA-AZ and AZ-MA Ox/Ox, the insulation performance in comparison to the MA and MA-MA system was reduced in both cases. However, the contribution of the lower thermally conductive mullite is still visible in the MA-dominated MA-AZ Ox/Ox. Hence, in contrast to the mechanical testing, it can be concluded that the thermal properties were mainly governed by the AZ matrix fraction in the composite.

Table 5
Sample thickness and density; thermal diffusivity α, specific heat capacity c_p and thermal conductivity λ at 1000 °C for all Ox/Ox systems.

	AZ	MA	AZ-AZ	MA-MA	AZ-MA	MA-AZ
t [mm]	1.94	1.78	1.95	1.96	1.95	2.08
ρ [g/cm³]	2.69	2.29	2.64	2.28	2.51	2.46
$\alpha_{1000\,°C}$ [mm²/s]	0.55	0.50	0.55	0.46	0.54	0.54
$c_{p\ 1000\,°C}$ [J/gK]	0.90	0.91	0.90	0.91	1.03	0.85
$\lambda_{1000\,°C}$ [W/mK]	1.35	1.05	1.32	0.96	1.40	1.13

3.4. Evaluation of the material concept

As the fabrication parameters chosen in this work could not provide composites with distinct separation between the inter- and intrabundle matrix, the postulated material concept could not be proved in its entirety. First, adjustments to the fabrication process must be made in order to avoid the commingling of both matrix phases. This might be achieved by higher drying temperatures or even pre-sintering after the first infiltration, yet with downsides regarding the drapability and the range of fiber volume content in the final composites. Mixing of intrabundle matrix phase in the interbundle regions could for example be counteracted by adding binder to the intrabundle matrix slurry and brushing off excessive slurry after the first infiltration step in a preconditioned state. Furthermore, if the second infiltration is performed with a slurry of higher solid loading, the redispersion of the intrabundle slurry might be diminished. Ultimately, reducing the targeted fiber volume content will reduce shear forces and thereby commingling of matrices during the lamination step.

Yet, there are still interesting findings, that can be yielded from the results obtained in this work. First, mixing of the matrices did lead to changes in the mechanical and thermal properties of the composite, that can be traced back to the new matrix composition. While the addition of zirconia to the MA matrix phase yielded composites of less strength and less damage-tolerance, which confirmed the expectations, the altered stress-strain-behavior after failure of the AZ-MA composite was somewhat surprising. A more detailed assessment of this behavior should be subject of a future work. Secondly, for the usage of different matrices within one composite and the combination of beneficial properties resulting thereof, one must consider possible mixing effects, that can partially or even fully diminish the desired effect. A distinct separation between inter- and intrabundle matrix is mandatory for the matrices to exhibit their respective beneficial properties in the composite. Hence, the optimization or adaption of matrix systems, that proved to work within the WMC concept, as well as the formulation of new systems, is not trivial.

4. Conclusion

Manufacturing of Ox/Ox by a single-step and sequential infiltration process was investigated with a focus on the mechanical and thermal properties of the resulting composites. Microstructural investigations revealed that the desired material concept of distinctly separated matrix phases inside and outside the fiber bundle (intra-/interbundle) was impaired by the shear-induced slurry flow in the laminate during the lamination process. This led to a comingling of the phases in the

interbundle and partially also in the intrabundle areas of the fabric layers, with the intrabundle matrix phase being dominant throughout the composite. As a result, mean values for the mechanical and thermal properties compared to the performance of Ox/Ox comprising solely one matrix phase were only observed for either the mechanical or the thermal properties. A somewhat unique stress-strain-relation after failure was detected for the infiltration sequence alumina-zirconia (1) and mullite-alumina (2) and might be attributed to the microstructure that resulted from the sintering between the mullite and zirconia particles within and around the fiber bundle. As the fabrication parameters chosen in this work could not provide the desired separation between inter- and intrabundle matrix phases in the composites, the postulated material concept remains to be proved in its entirety.

CRediT authorship contribution statement

Georg Puchas: Writing – review & editing, Writing – original draft, Visualization, Supervision, Resources, Project administration, Funding acquisition, Data curation. **Felix Lindner**: Writing – review & editing, Writing – original draft, Visualization, Validation, Methodology, Investigation, Formal analysis, Data curation, Conceptualization. **Sanaz Hariri**: Investigation. **Felix Wich**: Visualization, Investigation. **Stefan Schafföner**: Writing – review & editing, Supervision, Resources, Funding acquisition, Conceptualization.

Declaration of Competing Interest

The authors declare that they have no known competing financial interests or personal relationships that could have appeared to influence the work reported in this paper.

References

[1] F.W. Zok, Developments in oxide fiber composites, J. Am. Ceram. Soc. 89 (2006) 3309–3324, https://doi.org/10.1111/j.1551-2916.2006.01342.x.

[2] J.D. Kiser, N.P. Bansal, J. Szelagowski, J. (Jack) Sokhey, T. Heffernan, J. Clegg, A. Pierluissi, J. Riedell, T. Wyen, S. Atmur, J. Ursic, Oxide/Oxide Ceramic Matrix Composite (CMC) Exhaust Mixer Development in the NASA Environmentally Responsible Aviation (ERA) Project, in: ASME Turbo Expo Turbine Tech. Conf. Expo. Vol. 6 Ceram. Control. Diagnostics Instrumentation; Educ. Manuf. Mater. Metall. Honor. Award., American Society of Mechanical Engineers, 2015: pp. 1–15. https://doi.org/10.1115/GT2015-43593.

[3] C. Malinverni, M. Salvo, A. De Zanet, F. D'Isanto, F. Smeacetto, P. Bertrand, G. Puchas, S. Schafföner, V. Casalegno, Glass-ceramics for joining oxide-based ceramic matrix composites (Al2O3f/Al2O3-ZrO2) operating under direct flame exposure, J. Eur. Ceram. Soc. 43 (2023) 3621–3629, https://doi.org/10.1016/j.jeurceramsoc.2023.02.019.

[4] W. Pritzkow, A. Rüdinger, A. Nöth, Oxide Ceramic Matrix Composites – Manufacturing, Machining, Properties and Industrial Applications, Ceram. Appl. 3 (2015) 48–54.

[5] M.B. Ruggles-Wrenn, S. Mall, C.A. Eber, L.B. Harlan, Effects of steam environment on high-temperature mechanical behavior of NextelTM720/alumina (N720/A) continuous fiber ceramic composite, Compos. Part A Appl. Sci. Manuf. 37 (2006) 2029–2040, https://doi.org/10.1016/j.compositesa.2005.12.008.

[6] M.B. Ruggles-Wrenn, J.C. Braun, Effects of steam environment on creep behavior of Nextel™720/alumina ceramic composite at elevated temperature, Mater. Sci. Eng. A. 497 (2008) 101–110, https://doi.org/10.1016/j.msea.2008.06.036.

[7] C.J. Armani, M.B. Ruggles-Wrenn, G.E. Fair, R.S. Hay, Creep of Nextel™ 610 fiber at 1100°C in air and in steam, Int. J. Appl. Ceram. Technol. 10 (2013) 276–284, https://doi.org/10.1111/j.1744-7402.2012.02831.x.

[8] C.J. Armani, M.B. Ruggles-Wrenn, R.S. Hay, G.E. Fair, Creep and microstructure of Nextel™ 720 fiber at elevated temperature in air and in steam, Acta Mater 61 (2013) 6114–6124, https://doi.org/10.1016/j.actamat.2013.06.053.

[9] 3M Corporation, 3M Nextel Ceramic Fibers and Textiles: Technical Reference Guide, 2021.

[10] C.G. Levi, F.W. Zok, J.Y. Yang, M. Mattoni, J.P.A. Löfvander, Microstructural design of stable porous matrices for all-oxide ceramic composites, Zeitschrift Fuer Met. Res. Adv. Tech. 90 (1999) 1037–1047.

[11] A.G. Evans, F.W. Zok, The physics and mechanics of fibre-reinforced brittle matrix composites, J. Mater. Sci. 29 (1994) 3857–3896, https://doi.org/10.1007/BF00355946.

[12] M. Gerendás, Y. Cadoret, C. Wilhelmi, T. Machry, R. Knoche, T. Behrendt, T. Aumeier, S. Denis, J. Göring, D. Koch, K. Tushtev, Improvement of Oxide/Oxide CMC and Development of Combustor and Turbine Components in the HiPOC Program, in: Vol. 1 Aircr. Engine; Ceram. Coal, Biomass Altern. Fuels; Wind Turbine Technol., ASMEDC, 2011: pp. 477–490. https://doi.org/10.1115/GT2011-45460.

[13] E. Volkmann, K. Tushtev, D. Koch, C. Wilhelmi, J. Göring, K. Rezwan, Assessment of three oxide/oxide ceramic matrix composites: Mechanical performance and effects of heat treatments, Compos. Part A Appl. Sci. Manuf. 68 (2015) 19–28, https://doi.org/10.1016/j.compositesa.2014.09.013.

[14] E. Volkmann, L. Lima Evangelista, K. Tushtev, D. Koch, C. Wilhelmi, K. Rezwan, Oxidation-induced microstructural changes of a polymer-derived Nextel™ 610 ceramic composite and impact on the mechanical performance, J. Mater. Sci. 49 (2014) 710–719, https://doi.org/10.1007/s10853-013-7752-4.

[15] M. Frieß, S. Denis, Oxide CMC Components Manufactured via PIP Processing Based on Polysiloxanes, in: ECerS XII, 12th Conf. Eur. Ceram. Soc., Stockholm, 2011.

[16] C. Kaya, F. Kaya, E.G. Butler, A.R. Boccaccini, K.K. Chawla, Development and characterisation of high-density oxide fibre-reinforced oxide ceramic matrix composites with improved mechanical properties, J. Eur. Ceram. Soc. 29 (2009) 1631–1639, https://doi.org/10.1016/j.jeurceramsoc.2008.09.027.

[17] A.R. Boccaccini, S. Atiq, D.N. Boccaccini, I. Dlouhy, C. Kaya, Fracture behaviour of mullite fibre reinforced-mullite matrix composites under quasi-static and ballistic impact loading, Compos. Sci. Technol. 65 (2005) 325–333, https://doi.org/10.1016/j.compscitech.2004.08.002.

[18] Z. Chen, S. Duncan, K.K. Chawla, M. Koopman, G.M. Janowski, Characterization of interfacial reaction products in alumina fiber/barium zirconate coating/alumina matrix composite, Mater. Charact. 48 (2002) 305–314, https://doi.org/10.1016/S1044-5803(02)00279-6.

[19] R.J. Kerans, R.S. Hay, T.A. Parthasarathy, M.K. Cinibulk, Interface Design for Oxidation-Resistant Ceramic Composites, J. Am. Ceram. Soc. 85 (2004) 2599–2632, https://doi.org/10.1111/j.1151-2916.2002.tb00505.x.

[20] C.G. Levi, J.Y. Yang, B.J. Dalgleish, F.W. Zok, A.G. Evans, Processing and Performance of an All-Oxide Ceramic Composite, J. Am. Ceram. Soc. 81 (1998) 2077–2086, https://doi.org/10.1111/j.1151-2916.1998.tb02590.x.

[21] P.O. Guglielmi, G.F. Nunes, M. Hablitzel, D. Hotza, R. Janssen, Production of oxide ceramic matrix composites by a prepreg technique, 727–728, Mater. Sci. Forum. (2012) 556–561, https://doi.org/10.4028/www.scientific.net/MSF.727-728.556.

[22] R.S.M. Almeida, T.F.S. Pereira, K. Tushtev, K. Rezwan, Obtaining complex-shaped oxide ceramic composites via ionotropic gelation, J. Am. Ceram. Soc. 102 (2019) 53–57, https://doi.org/10.1111/jace.15990.

[23] R.A. Simon, Progress in processing and performance of porous-matrix oxide/oxide composites, Int. J. Appl. Ceram. Technol. 2 (2005) 141–149, https://doi.org/10.1111/j.1744-7402.2005.02016.x.

[24] B. Kanka, H. Schneider, Aluminosilicate fiber/mullite matrix composites with favorable high-temperature properties, J. Eur. Ceram. Soc. 20 (2000) 619–623, https://doi.org/10.1016/S0955-2219(99)00260-5.

[25] L.P. Zawada, R.S. Hay, S.S. Lee, J. Staehler, Characterization and high-temperature mechanical behavior of an oxide/oxide composite, J. Am. Ceram. Soc. 86 (2003) 981–990, https://doi.org/10.1111/j.1151-2916.2003.tb03406.x.

[26] X. Chen, H. Liu, R. Jiang, X. Sun, Microstructure, mechanical properties and thermal shock behavior of 2.5D oxide fiber preform reinforced oxide matrix composites, Ceram. Int. 50 (2024) 17020–17033, https://doi.org/10.1016/j.ceramint.2024.02.179.

[27] R.A. Jurf, S.C. Butner, Advances in Oxide-Oxide CMC, J. Eng. Gas Turbines Power. 122 (2000) 202–205, https://doi.org/10.1115/1.483195.

[28] Y. Shi, S. Hönig, M. Frieß, A. Rüdinger, W. Pritzkow, D. Koch, Manufacture and characterization of oxide ceramic matrix composites out of commercial pre-impregnated fabrics, Ceram. Int. 44 (2018) 2320–2327, https://doi.org/10.1016/j.ceramint.2017.10.198.

[29] G. Puchas, S. Möckel, W. Krenkel, Novel prepreg manufacturing process for oxide fiber composites, J. Eur. Ceram. Soc. 40 (2020) 5930–5941, https://doi.org/10.1016/j.jeurceramsoc.2020.06.064.

[30] Z. Borius, A. Débarre, M. Singlard, T. Cutard, A. Julian-Jankowiak, Impact of additives on the quality of oxide/oxide tow-pregs obtained by continuous fibre impregnation, Compos. Part A Appl. Sci. Manuf. 184 (2024), https://doi.org/10.1016/j.compositesa.2024.108238.

[31] M. Fritsch, H. Klemm, M. Herrmann, B. Schenk, Corrosion of selected ceramic materials in hot gas environment, J. Eur. Ceram. Soc. 26 (2006) 3557–3565, https://doi.org/10.1016/j.jeurceramsoc.2006.01.015.

[32] A. Otsuka, Y. Waku, K. Kitagawa, N. Aral, Effect of hot corrosive environment on ceramics, Energy 30 (2005) 523–533, https://doi.org/10.1016/j.energy.2004.04.018.

[33] M.J. Presby, N. Kedir, L.J. Sanchez, C. Gong, D. Faucett, S.R. Choi, G.N. Morscher, Erosion Behavior in a Gas Turbine Grade Oxide/Oxide Ceramic Matrix Composite, in: Proc. 42nd Int. Conf. Adv. Ceram. Compos. Ceram. Eng. Sci., 2019: pp. 15–25. https://doi.org/10.1002/9781119543343.ch2.

[34] P. Mechnich, Slurry-based protective coatings for Oxide/Oxide ceramic matrix composites, J. Ceram. Soc. Japan. 129 (2021) 32–39, https://doi.org/10.2109/jcersj2.20166.

[35] F.W. Zok, C.G. Levi, Mechanical Properties of Porous-Matrix Ceramic Composites, Adv. Eng. Mater. 3 (2001) 15–23, https://doi.org/10.1002/1527-2648(200101)3:1/2<15::AID-ADEM15>3.0.CO;2-A.

[36] E.A.V. Carelli, H. Fujita, J.Y. Yang, F.W. Zok, Effects of Thermal Aging on the Mechanical Properties of a Porous-Matrix Ceramic Composite, J. Am. Ceram. Soc. 85 (2002) 595–602, https://doi.org/10.1111/j.1151-2916.2002.tb00138.x.

[37] G. Puchas, A. Held, W. Krenkel, Near-net shape manufacture process for oxide fiber composites (OFC), Mater. Today Proc. 16 (2019) 49–58, https://doi.org/10.1016/j.matpr.2019.05.278.

[38] L. Wagner, G. Puchas, W. Krenkel, S. Schafföner, Influence of matrix densification on the properties of weak matrix oxide fiber composites, Compos. Part A Appl. Sci. Manuf. 164 (2023) 107274, https://doi.org/10.1016/j.compositesa.2022.107274.
[39] G. Puchas, S. Möckel, W. Krenkel, Novel prepreg manufacturing process for oxide fiber composites, J. Eur. Ceram. Soc. 40 (2020) 5930–5941, https://doi.org/10.1016/j.jeurceramsoc.2020.06.064.
[40] J. Winkelbauer, G. Puchas, W. Krenkel, S. Schafföner, Short fiber spraying process of all-oxide ceramic matrix composites: A parameter study, Int. J. Appl. Ceram. Technol. (2022), https://doi.org/10.1111/ijac.14196.
[41] J. Winkelbauer, G. Puchas, S. Schafföner, W. Krenkel, Short fiber-reinforced oxide fiber composites, Int. J. Appl. Ceram. Technol. 19 (2022) 1136–1147, https://doi.org/10.1111/ijac.13931.
[42] E. Galiev, R. Trân, S. Winter, F. Lindner, G. Puchas, C. Wüstner, M. Thomas, S. Knohl, V. Psyk, S. Schafföner, W. Krenkel, V. Kräusel, Hybrid ceramic insulation made of oxide fiber ceramic matrix composite and paper-based ceramic for hot forming tools, Open Ceram 15 (2023) 100403, https://doi.org/10.1016/j.oceram.2023.100403.
[43] S. Schafföner, C.G. Aneziris, Pressure slip casting of coarse grain oxide ceramics, Ceram. Int. 38 (2012) 417–422, https://doi.org/10.1016/j.ceramint.2011.06.064.
[44] S. Schafföner, L. Freitag, J. Hubálková, C.G. Aneziris, Functional composites based on refractories produced by pressure slip casting, J. Eur. Ceram. Soc. 36 (2016) 2109–2117, https://doi.org/10.1016/j.jeurceramsoc.2016.02.008.
[45] F. Lindner, G. Puchas, S. Schafföner, Novel measuring method for prepreg processability of oxide fiber ceramic matrix composites, Compos. Part A Appl. Sci. Manuf. 162 (2022) 107131, https://doi.org/10.1016/j.compositesa.2022.107131.
[46] B. Chen, T.W. Chou, Compaction of woven-fabric preforms: Nesting and multi-layer deformation, Compos. Sci. Technol. 60 (2000) 2223–2231, https://doi.org/10.1016/S0266-3538(00)00017-8.
[47] F. Zok, F.F. Lange, J.I. Porter, Packing Density of Composite Powder Mixtures, J. Am. Ceram. Soc 74 (1991) 1880–1885, https://doi.org/10.1007/springerreference_20874.
[48] J. Lincoln, B. Jackson, A. Barnes, A.R. Beaber, L. Visser, Oxide-Oxide Ceramic Matrix Composites - Enabling Widespread Industry Adoption, in: M. Singh, T. Ohji, S. Dong, D. Koch, K. Shimamura, B. Clauss, B. Heidenreich, J. Akedo (Eds.), Adv. High Temp. Ceram. Matrix Compo Sites Mater. Sustain. Dev. Ceram. Trans. Vol. CCLXIII, Vol. 263, First Ed., 1st ed., 2017: pp. 401–412. https://doi.org/10.1002/9781119407270.ch38.
[49] E. Volkmann, A. Dentel, K. Tushtev, C. Wilhelmi, K. Rezwan, Influence of heat treatment and fiber orientation on the damage threshold and the fracture behavior of Nextel fiber-reinforced Mullite-SiOC matrix composites analysed by acoustic emission monitoring, J. Mater. Sci. 49 (2014) 7890–7899, https://doi.org/10.1007/s10853-014-8501-z.
[50] M.G. Holmquist, F.F. Lange, Processing and Properties of a Porous Oxide Matrix Composite: Reinforced with Continuous Oxide Fibers, J. Am. Ceram. Soc. 86 (2003) 1733–1740, https://doi.org/10.1111/j.1151-2916.2003.tb03548.x.